Fei Qin
Institute of Electronics Packaging Technology and Reliability,
Faculty of Materials and Manufacturing,
Beijing University of Technology,
Beijing 100124, China;
Beijing Key Laboratory of Advanced Manufacturing Technology,
Faculty of Materials and Manufacturing,
Beijing University of Technology,
Beijing 100124, China

Qi He
Institute of Electronics Packaging Technology and Reliability,
Faculty of Materials and Manufacturing,
Beijing University of Technology,
Beijing 100124, China

Yanpeng Gong[1]
Institute of Electronics Packaging Technology and Reliability,
Faculty of Materials and Manufacturing,
Beijing University of Technology,
Beijing 100124, China;
Beijing Key Laboratory of Advanced Manufacturing Technology,
Faculty of Materials and Manufacturing,
Beijing University of Technology,
Beijing 100124, China
e-mail: yanpeng.gong@bjut.edu.cn

Chuantao Hou
Science and Technology on Reliability and Environment Engineering Laboratory,
Beijing Institute of Structure and Environment Engineering,
Beijing 100076, China

Hao Cheng
Science and Technology on Reliability and Environment Engineering Laboratory,
Beijing Institute of Structure and Environment Engineering,
Beijing 100076, China

Tong An
Institute of Electronics Packaging Technology and Reliability,
Faculty of Materials and Manufacturing,
Beijing University of Technology,
Beijing 100124, China;
Beijing Key Laboratory of Advanced Manufacturing Technology,
Faculty of Materials and Manufacturing,
Beijing University of Technology,
Beijing 100124, China

An Automatic Finite Element Method-Boundary Element Method Coupling Method for Elastic–Plastic Problems of Multiscale Structures in Electronic Packaging

We introduce a coupled finite and boundary element method for elastic-plastic analysis over multiscale electronic packaging structures. Based on the finite element-boundary element (FE-BE) coupling algorithm, an automatic implementation procedure for the coupling of the ABAQUS with a self-written elastic BE code is introduced for elastic problems. In the mixed finite element method (FEM)-boundary element method (BEM) model, the effective stiffness and effective forces at the interfacial boundary are evaluated by the self-written BE code. Then, the obtained effective stiffness and effective forces are assembled to the global FE formulations by using the user subroutine (UEL) in ABAQUS. Numerical simulation of structures with plastic deformation, stress concentration, etc. is carried out by using FEM theory. The boundary element method is used for linear elastic domains with large-scale structures. The proposed method offers several key improvements compared with current analysis methods available for multiscale electronic packaging structures. The benefits are: (i) the powerful pre- and postprocessing of ABAQUS; (ii) the higher accuracy of the solution; (iii) the computational cost and time can be reduced by using the scheme; and (iv) solving systems with infinite extension by using the BEM as a supplement. Furthermore, we demonstrate the ability of the proposed approach to handle multiscale structures in electronic packaging problems. [DOI: 10.1115/1.4055125]

Keywords: boundary element method, finite element method, coupling method, ABAQUS, elasic problems with multiscale structures

[1]Corresponding author.

Contributed by the Electronic and Photonic Packaging Division of ASME for publication in the JOURNAL OF ELECTRONIC PACKAGING. Manuscript received April 5, 2022; final manuscript received July 22, 2022; published online August 18, 2022. Assoc. Editor: Ming-Yi Tsai.

Yanwei Dai
Institute of Electronics Packaging Technology and Reliability,
Faculty of Materials and Manufacturing,
Beijing University of Technology,
Beijing 100124, China;
Beijing Key Laboratory of Advanced Manufacturing Technology,
Faculty of Materials and Manufacturing,
Beijing University of Technology,
Beijing 100124, China

Pei Chen
Institute of Electronics Packaging Technology and Reliability,
Faculty of Materials and Manufacturing,
Beijing University of Technology,
Beijing 100124, China;
Beijing Key Laboratory of Advanced Manufacturing Technology,
Faculty of Materials and Manufacturing,
Beijing University of Technology,
Beijing 100124, China

1 Introduction

With the rapid development of advanced electronic systems, electronic packaging which plays the role of support and protection in integrated circuits gets more and more important [1]. However, during the operation of the electronic device, a lot of heat will be generated due to the resistance to the current transmitted through the transistors, thus generating a significant temperature gradient on each packaged component. The presence of temperature gradient brings challenges to the reliability of electronic devices. Therefore, the long-term packaging reliability is becoming one of the key requirements for the design of electronic packaging structures.

With characteristics of easy implementation, saving resources, no environmental restriction, etc., the simulation-based design for electronic packaging structures is becoming the mainstream technique. Currently, various programs, focused on mechanics reliability analysis and based on the finite element method (FEM), are available (i.e., ABAQUS, ANSYS, COMSOL, etc.) [2–4]. In Ref. [5], Cheng et al. constructed a three-dimensional (3D) through-silicon via (TSV) stacked-chips packages model by the commercial software ANSYS to investigate the thermo-mechanical behavior for packages stressed under temperature cycle test. It's obvious that there are many large-scale parts and small-scale parts in TSV model, which increased the number of elements and the computing time greatly. Zhang et al. [6] investigated the impact reliability of a microsystem based on rigid-flex printed circuit board using the commercial ABAQUS/EXPLICIT solver and determined the relationship between the stress distribution and the layout of the rigid circuit boards. In Ref. [7], the vibration reliability of lead-free solder joints of package-on-package is investigated by using FEM and verified by experimental tests. The authors developed a finite element model and analyzed the natural frequencies and modes by FEM.

From these works, we can find that the FEM plays an important role in the simulation analysis of electronic packaging structure. However, due to the multiscale structures in the electronic packaging, the numerical model must be discretized into plenty of elements to ensure the calculation accuracy, which has increased the computational time and cost. To solve this problem, the boundary element method is extended and used to analyze electronic packaging problems. In Ref. [8], Yu et al. presented a boundary element method (BEM) to study the heat transfer problems of electronic packaging structures. Since advantages of reduction dimensionality of the problem by one, only boundary discretization required and high accurate stress analysis, BEM seems to be a promising method in packaging reliability for electronic devices. Vallepuga-Espinosa et al. [9] used BEM to study the thermoelastic contact problem of micro-electronic packaging with low heat generation. By using the BEM, the values of the final thermal and mechanical variables of the micro-electronic packaging and the thermal contact resistance are obtained with a small number of boundary elements. In Ref. [10], Khatir et al. present an analysis method based on the boundary element method (BEM) to investigate thermal behavior of high power semiconductor packages subjected to power cycling loads. The BEM was used to carry out stress analysis of integrated circuit packages under the remote loading or the pressure acting on the delamination surfaces by Dong and Lee [11]. Fundamental solutions derived from symmetrical property of the problems were adopted to further reduce the number of elements used in the discretization of the problem boundary. The authors found that the BEM can produce accurate numerical results for the analysis of electronic packaging problems. The advantages of BEM can be summarized as follows. (i) The reduction of dimensionality by one, which is a direct result of the 'surface-only' modeling. (ii) Stresses are exact (and fully continuous) inside the domain because no further approximation is imposed on the solution at interior points. (iii) Compared with other schemes, BEM needs less computer time and storage for the same level of accuracy.

Although the number of elements can be largely reduced by BEM in the analysis of complex electronic packaging structures, the BEM is not a preferable approach for the complicated nonlinear and nonhomogeneous problems. Therefore, a large research community proposed the coupling scheme to use the best features of FEM and BEM. In 1977, Zienkiewicz and Bettess [12] first introduced how the BEM can be utilized in conventional FEM context. Then, the initial work attracted a large research community and the coupling scheme expanded rapidly from heat transfer problems [12] to many other applications, including fluid–structure interaction [13–15], acoustic problems [16,17], magnetostatic field problems [18–21], soil and rock [22–24], etc.

Actually, most of the early coupling schemes are implemented by noncommercial (or self-written) code packages. With the development of FEM, the commercial software is more and more preferred due to its powerful pre/postprocessing capabilities. Therefore, lots of coupling scheme based on commercial FEM software are developed. In Ref. [25], Liu and Dong coupled the self-written linear elastic boundary element code to the commercial finite element system ABAQUS by using the user-defined element (UEL) subroutine. Sharma et al. [26] analyzed the acoustic radiation characteristic of vibrating laminated composite conical shell panels by using the coupled FEM-BEM technique. Helldorfer et al. [27] presented an automatic procedure for the coupling of FEM and BEM. The coupling procedure was implemented using the inhouse symmetric Galerkin boundary element method code and the commercial finite element package ABAQUS. Actually, the FEM and BEM coupling method has been successfully implemented using the built-in UEL subroutine in ABAQUS. More details about the coupling scheme are given in Refs. [25], [27], and [28].

In this paper, we will develop a FEM-BEM coupling scheme to analyze the mechanical problems in electronic packaging. Since the user element implementation in the ABAQUS permits the element to function in a way similar to any standard ABAQUS finite element, the boundary element region is treated as a "finite element" and incorporated into ABAQUS by user subroutine. In the implementation of the current coupling scheme, the considered model will be divided into two parts: the finite element (FE) subdomain and boundary element (BE) subdomain. It should be noted that the subdomain with nonlinear or inhomogeneous behavior will be deemed as the FE subdomain and solved by ABAQUS. BEM will be used to solve the subdomain with linear behavior (or unimportant areas). It is for this reason that, when we use BEM to analyze these regions, only the boundary information or quantities are needed and the number of degree-of-freedom can be largely reduced. What's more, the accuracy of the numerical results can be guaranteed due to the features of BEM. Then, the interface between the FE subdomain and BE subdomain (a line element for two-dimensional (2D) model and a surface element for 3D model) will be treated as "super-elements" [29]. Here, the super-elements are equivalent to the user-defined elements built in ABAQUS. The self-written BE code will be started inside UEL to get the effective stiffness and effective nodal forces for the user-defined elements. Then, the FE subdomain can be solved by using ABAQUS.

This paper is organized as follows: In Sec. 2, some fundamental formulations about FEM and BEM are given. Section 3 presents the implementation of the coupling scheme for elasticity. The process of coupling ABAQUS and the self-written BEM code is presented in Sec. 4. Some numerical examples are analyzed in Sec. 5 to demonstrate the correctness and efficiency of the coupled method. Finally, some conclusions are given in Sec. 6.

2 Fundamental Formulations for Finite Element Method and Boundary Element Method

2.1 Finite Element Formulations. Consider a 2D solid model occupying Ω, in which the internal stresses $\{\sigma\}$, the distributed volume force $\{f\}$ and the external applied tractions $\{t\}$ form an equilibrating field. The total potential energy Π_p of the system is given as [30,31]

$$\Pi_p = \frac{1}{2}\int_\Omega \{\varepsilon\}^T\{\sigma\}d\Omega - \int_\Omega \{d\}^T\{f\}d\Omega - \int_\Gamma \{d\}^T\{t\}d\Gamma \quad (1)$$

where $\{\varepsilon\}$ and $\{d\}$ represent the strain tensor and internal displacement tensor, respectively. Ω and Γ denote the computational domain and its boundary.

By the use of the total potential energy principle, the final systems of the assembled finite element equations in elasticity are written as [30,31]

$$[K]\{u\} = \{F\} \quad (2)$$

2.2 Boundary Element Formulations for Elastic Problems. Boundary element method is an efficient and powerful tool to solve boundary value problems in linear elasticity, see, e.g., Refs. [32–34], in which the governing partial differential equation is reformulated as a boundary integral equation allowing the computational model to be restricted to the boundary only. This section focuses on showing the methodology of BEM for plane elasticity. More formulations about BEM are given in the original papers [33,34] written by Chen and Hong. Let Ω be a bounded domain with boundary Γ, in which the corresponding boundary integral equation can be written as

$$c_{ij}(\mathbf{y})u_j(\mathbf{y}) + \int_\Gamma t^*_{ij}(\mathbf{x},\mathbf{y})u_j(\mathbf{x})d\Gamma(x) = \int_\Gamma u^*_{ij}(\mathbf{x},\mathbf{y})t_j(\mathbf{x})d\Gamma(\mathbf{x}) \quad (3)$$

where $\mathbf{x} \in \Gamma$ and $\mathbf{y} \in \Gamma$ are called the source point and field point, respectively. Subscripts $i, j = 1, 2$ denote the coordinate directions in 2D problems. u^*_{ij} and t^*_{ij} are the displacement and traction fundamental solutions. c_{ij} is the jump term which is commonly calculated indirectly by using a simple physical consideration. The displacement fundamental solutions in 2D for isotropic materials are given as

$$u^*_{ij} = \frac{1}{8\pi(1-\nu)\mu}\left[(3-4\nu)\delta_{ij}\ln\left(\frac{1}{r}\right) + r_{,i}r_{,j}\right] \quad (4)$$

where μ and ν are the shear modulus and Poisson's ratio, respectively. r is the distance between the source point and field point, i.e.,

$$r = r(\mathbf{x},\mathbf{y}) = \sqrt{(y_i - x_i)(y_i - x_i)} \quad (5)$$

in which the summation convention is used. The normal derivative of displacement fundamental solutions t^*_{ij} are given as

$$t^*_{ij} = \frac{-1}{4\pi(1-\nu)r}\left\{\left[(1-2\nu)\delta_{ij} + 2r_{,i}r_{,j}\right]\frac{\partial r}{\partial \mathbf{n}} - (1-2\nu)(r_{,i}n_j - r_{,j}n_i)\right\} \quad (6)$$

$r_{,i} = \frac{\partial r}{\partial x_i}$, and n_i is the ith component of the unit outward normal vector $\mathbf{n}$ to the boundary.

In the implementation of BEM, the boundary Γ may thus be considered to be divided into elements Γ_e, $e = 1, 2, \ldots, N_e$. The displacement and traction components around the boundary can be expressed by using the interpolation functions, i.e.,

$$u(\xi) = \sum_{i=1}^{n} N_i(\xi)\tilde{u}_i \quad (7)$$

$$t(\xi) = \sum_{i=1}^{n} N_i(\xi)\tilde{t}_i \quad (8)$$

where $\tilde{u}_i$ and $\tilde{t}_i$ are the local displacement and traction associated with the nodal point with index i; ξ is the local coordinates and n represents the number of nodal points for each element; $N_i(\xi)$ is the interpolation function.

Replacing the continuous functions u and t by the expansions in Eqs. (7) and (8), the boundary integral equation in Eq. (3) is written in a Discretized form:

$$c_{ij}(\xi_c)u_j(\xi_c) + \sum_{e=1}^{N_e}\sum_{j=1}^{n}\left[\int_{-1}^{1} t^*_{ij}(\xi,\xi_c)N_j(\xi)d\xi\right]u^e_j = \sum_{e=1}^{N_e}\sum_{j=1}^{n}\left[\int_{-1}^{1} u^*_{ij}(\xi,\xi_c)N_j(\xi)d\xi\right]t^e_j \quad (9)$$

If the discretized boundary integral equation is applied consecutively for all the source points located at the boundary Γ, the

Eq. (9) can be assembled into a system of linear algebraic equations, i.e.,

$$\mathbf{Hu} = \mathbf{Gt} \tag{10}$$

where $\mathbf{u}$ and $\mathbf{t}$ represent the vectors containing the nodal displacements and tractions, respectively. $\mathbf{H} = [H_{ij}]$ and $\mathbf{G} = [G_{ij}]$ denote the coefficient matrix with

$$H_{ij} = \int_{-1}^{1} t_{ij}^{*}(\xi, \xi_c) N_j(\xi) d\xi \tag{11}$$

and

$$G_{ij} = \int_{-1}^{1} u_{ij}^{*}(\xi, \xi_c) N_j(\xi) d\xi \tag{12}$$

2.3 Boundary Element Method for Multiple Domains. For the multiple domain cases where we have layers or zones of different materials, special solution methods based on the fundamental solutions for homogeneous materials might be adopted. Each region is treated in the same way as discussed previously but can now be assigned different material properties. It should be pointed out that since at the interfaces between different regions both displacement $\mathbf{u}$ and traction $\mathbf{t}$ are not known, the number of unknowns will be increased. Additional equations including the conditions of equilibrium and compatibility at the interfaces are required to solve these problems. In this work, an assembly procedure that is similar to the approach taken by the finite element method is used [35]. We construct a stiffness matrix $\mathbf{K}$ for BEM, of each domain, the coefficients of which are the tractions under unit displacements. The matrices $\mathbf{K}$ for all domains are then assembled in the same way as with the finite element method. This assembly procedure is efficient and amenable to implementation on coupling boundary with finite element method as outlined in Secs. 2.3.1 and 2.3.2.

The assembly procedure used in this work is explained in detail on a simple example (shown in Figs. 1(*a*) and 1(*b*)) for elasticity problem.

2.3.1 Stiffness Matrix K^N for Fully Coupled Problems. Consider the model in Fig. 1(*a*), the region II is completely covered by region I, and the outward normals of the two regions point in directions opposite to each other. In this work, we call this kind of coupled case as fully coupled problems. To solve the problem with two regions, the "stiffness matrix $\mathbf{K}^N$" for each region $N\,(=\mathrm{I}, \mathrm{II})$ should be computed. Coefficients of $\mathbf{K}^N$ are values of nodal tractions $\mathbf{t}$ due to unit values of displacements $\mathbf{u}$ at all nodes in turn. The first column of $\mathbf{K}^N$ can be obtained by applying a unit value of displacement in $i\,(i = 1, 2)$ direction at a node and set all other node values to 0. Therefore, we can obtain the stiffness matrix $\mathbf{K}^N$ of a domain by solving a Dirichlet problem M times (M represents the number of degrees-of-freedom of the BE region).

For the implementation of 2D Dirichlet problem, the $i = 1$ direction of the first node is subjected to the unit displacement, i.e., $u_1^1 = 1$. The $i = 2$ direction of the first node and all the directions of other nodes are subjected to 0 displacement. Then, vector u^1 is written as

For the implementation of 2D Dirichlet problem, the $i = 1$ direction of the first node is subjected to the unit displacement ($u_1^1 = 1$). While the $i = 2$ direction of the first node and all the directions of other nodes are subjected to 0 displacement. Then, vector $\mathbf{u}^1$ is written as

$$\mathbf{u}^1 = [1, 0, \ldots, 0]^T \tag{13}$$

By substituting Eq. (13) to Eq. (10), it follows that:

$$\mathbf{Gt}^1 = \mathbf{Hu}^1 \tag{14}$$

where $\mathbf{Hu}^1$ is the first column of $\mathbf{H}$ and represented by $\mathbf{F}^1$. Therefore, the stiffness matrix can be computed by solving the systems in Eq. (14) by applying all the displacement vectors $\mathbf{u}^i (i = 1, 2, \ldots, n)$, where n is the number of degree-of-freedom. Here, $\mathbf{u}^i$ is a vector with the ith value equalling 1. Each unknown traction vector $\mathbf{t}^i$ in Eq. (14) represents a column in $\mathbf{K}$, i.e.,

$$\mathbf{K} = [\mathbf{t}^1, \mathbf{t}^2, \ldots, \mathbf{t}^n] \tag{15}$$

2.3.2 Interfacial Stiffness Matrix $\mathbf{K}^N$ for Partially Coupled Problems. Consider the model in Fig. 1(*b*), which contains two homogeneous domains (I and II). In this model, not all the nodes of the regions are connected. Thus, we call this problem as partially coupled problems. As is shown in Fig. 1(*b*), the displacements at boundary Γ_u are fixed. A pressure is subjected to Γ_t. To solve the problem with two regions, the stiffness matrix $\mathbf{K}^N$ for each region $N\,(=\mathrm{I}, \mathrm{II})$ should be computed. For these problems, two types of problems need to be solved. We first solve a problem with zero values of displacements $\mathbf{u}$ at the interface between two regions and then solve the problem where unit values of $\mathbf{u}$ are applied at each node in turn.

Step 1: Evaluation of $\{t_{a^0}^N\}$.

The nodes at interface are subjected to the Dirichlet boundary condition with zero prescribed values $\mathbf{u}_a = 0$. For nodes that are not connected to other regions, the original boundary conditions are applied. Then, the system equation for each domain N can be written as

$$\begin{bmatrix} H_{a^0}^N & H_{b^0}^N \end{bmatrix} \begin{Bmatrix} u_{a^0}^N \\ u_{b^0}^N \end{Bmatrix} = \begin{bmatrix} G_{a^0}^N & G_{b^0}^N \end{bmatrix} \begin{Bmatrix} t_{a^0}^N \\ t_{b^0}^N \end{Bmatrix} \tag{16}$$

where the subscripts a^0 and b^0 represent the quantities at the interface and noninterface, respectively. The unknown interface traction $\{t_{a^0}^N\}$ (at the coupled nodes) and other physical quantities $\mathrm{x}_{f^0}^N$ can be obtained by solving the following equation

$$B^N \begin{bmatrix} t_{a^0}^N \\ x_{f^0}^N \end{bmatrix} = F_0^N \tag{17}$$

where matrix $\mathbf{B}^N$ is the assembled left-hand side and vector $\mathbf{F}_0^N$ contains the right-hand side. The vector $\mathbf{x}_{f^0}$ contains either displacements or tractions at the free nodes of the corresponding region.

Step 2: Evaluation of interfacial stiffness matrix K_B^N.

In this step, Dirichlet problem subjected to a unit displacement value at the ith direction of each of the interface nodes in turn will be solved. For free nodes, zero prescribed displacement values are used. The system equation of each region can be written as

$$\begin{bmatrix} H_{c_n}^N & H_{f_n}^N \end{bmatrix} \begin{Bmatrix} u_{c_n}^N \\ u_{f_n}^N \end{Bmatrix} = \begin{bmatrix} G_{c_n}^N & G_{f_n}^N \end{bmatrix} \begin{Bmatrix} t_{c_n}^N \\ t_{f_n}^N \end{Bmatrix} \tag{18}$$

where vector $\{u_{c_n}\}$ and $\{t_{c_n}\}$ represent the displacement and traction at the coupled nodes, respectively. $n = 1, 2, \ldots, N_c$, N_c is the number of interface degrees-of-freedom. $\{u_{f_n}\}$ and $\{t_{f_n}\}$ are the displacement and traction at the free nodes. Based on the known quantities, Eq. (18) can be expressed as

$$B^N \begin{bmatrix} \mathbf{t}_{cn}^N \\ \mathbf{x}_{fn}^N \end{bmatrix} = \mathbf{F}_n^N \tag{19}$$

where $\mathbf{F}_n^N$ is the right-hand side computed for a unit value of u at node n. $\mathbf{t}_{cn}^N$ is the traction at the coupled nodes. $\mathbf{x}_{fn}^N$ contains the

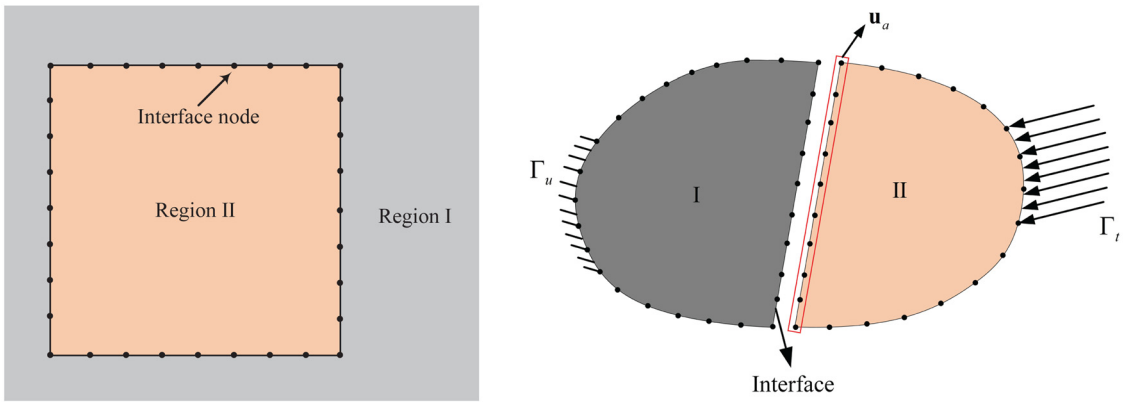

Fig. 1 Multiregion analysis models: (*a*) fully coupled problem and (*b*) partially coupled problem

displacement or traction at the free nodes when the unit Dirichlet boundary condition is applied at node n. $\mathbf{B}^N$ is the left-hand side of the system of equations. $\mathbf{F}_n$ is a vector corresponding to the nth column of $\mathbf{H}$ in Eq. (14).

The relationship between displacements and traction at interface can be expressed as

$$\mathbf{t}_c^N = \left\{t_{c_0}^N\right\} + \left[K_B^N\right]\left\{u_c^N\right\} \tag{20}$$

where $\left\{u_c^N\right\}$ containing the displacements at the interface nodes of region N and the stiffness matrices $\mathbf{K}_B^N$ is defined by

$$\mathbf{K}_B^N = \left[\{t_{c_1}\}\{t_{c_2}\}\cdots\{t_{c_{N_c}}\}\right]^N \tag{21}$$

Since the equations of compatibility or preservation of displacement and traction at the interface can be written as

$$\mathbf{t}_c^I + \mathbf{t}_c^{II} = 0;\ \mathbf{u}_c^I = \mathbf{u}_c^{II} \tag{22}$$

Substituting Eq. (22) into Eq. (20) we obtain

$$\mathbf{K}\mathbf{u}_c + \mathbf{F} = 0 \tag{23}$$

where $\mathbf{K}$ is the assembled "stiffness matrix" of the interface nodes and $\mathbf{F}$ is the assembled right-hand side. By solving the above Eq. (23), the unknown interface displacements $\mathbf{u}_c$ at the nodes are obtained. Therefore, the unknown interface tractions $\mathbf{t}_c$ at the nodes can be obtained by Eq. (20). Finally, the calculation of all the unknowns at free nodes can be done separately for each region by Eq. (10).

3 Linking of Finite Element Method With Boundary Element Method

In general, there are two kinds of schemes for coupling the BEM and FEM. In the first scheme, the BE domain is treated as a large finite element. After the stiffness matrix $\mathbf{K}_{BE}$ of BEM being computed, the matrix is assembled into the global stiffness matrix $\mathbf{K}_{FE}$ of finite element. For the second approach, finite elements are treated as equivalent BE domain. Then the stiffness matrix $\mathbf{K}_{BE}$ can be determined and assembled as explained in Secs. 2.3.1 and 2.3.2 for multiple domains. In this work, the first approach is adopted to realize the coupling procedure. In the following, we will give a brief introduction to the theoretical basis and implementation of the first approach. More details about the coupling scheme are given in Ref. [35].

For the finite element method, the resulted system of equations has related the displacements at all the nodes to nodal forces. In the BEM, a relationship between nodal displacements and nodal tractions is established, which is different from the quantities in finite element method. Hence, to couple BEM to FEM, the surface tractions $\mathbf{t}_c$ (in BEM) should be converted into equivalent nodal forces $\mathbf{F}_c$ used in FEM. Consider the model in Fig. 2, consisting of one BE region and one FE region. For an element e, we apply an arbitrary virtual displacement δu_x^e in x-direction at a node along the interface element e. Then, the work obtained by nodal forces F_x can be written as

$$\delta W_x^{(e)} = (\delta u_x^e)F_x = \sum_{i=1}^{n}\left[(F_x)_i(\delta u_x^e)_i\right] \tag{24}$$

where n represents the number of nodes for an element.

For equilibrium to be satisfied, the work done by the surface traction (t_x) equals that done by the equivalent nodal forces (F_x), which gives

$$\delta W_x^{(e)} = \int_{\Gamma_e}(t_x\delta u_x)d\Gamma \tag{25}$$

For element e, the tractions and displacements can be easily interpolated as

$$\delta u_x = \sum_{i=1}^{n} N_i\delta(u_x^e)_i \tag{26}$$

$$t_x = \sum_{j=1}^{n} N_j(t_x^e)_j \tag{27}$$

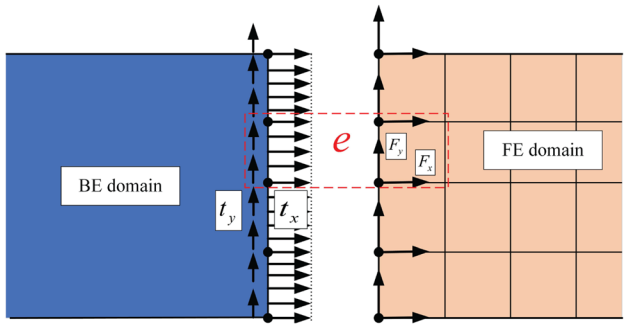

Fig. 2 Interface between FE and BE regions showing interface forces

From Eqs. (24)–(27), we can obtain that

$$(F_x)_i = \sum_{j=1}^{n} (t_x)_i \int_{\Gamma_e} N_i N_j d\Gamma \tag{28}$$

A similar equation can be obtained by applying virtual displacement in y-direction, which can be shown as

$$(F_y)_i = \sum_{j=1}^{n} (t_y)_i \int_{\Gamma_e} N_i N_j d\Gamma \tag{29}$$

The boundary integral on the right-hand side of Eqs. (28) and (29) can be evaluated by using a regular Gauss quadrature.

Let

$$[M^e] = \sum_{j=1}^{n} \int_{\Gamma_e} N_i N_j d\Gamma \tag{30}$$

the relationship between surface tractions and equivalent nodal forces can be expressed as

$$[F_c] = [M]\{t_c\} \tag{31}$$

where $\mathbf{F}_c$ is nodal forces at the interface. Matrix $\mathbf{M}$ which is assembled by $\mathbf{M}^e$ denotes transformation matrix for the whole interface.

Then, Eq. (20) can be expressed in terms of equivalent nodal point forces by premultiplying with the matrix $[M]$

$$\{F_c\} = [M]\{t_c^N\} = [M]\left\{t_{c_0}^N\right\} + [M][K_B^N]\{u_c^N\} \tag{32}$$

where $[M]\{t_c^N\}$ is the effective initial nodal force and written as $F_{c_0}^B$; MK_B^N denotes the effective stiffness matrix and written as $K_{c_0}^B$. Here, the $K_{c_0}^B$ becomes a stiffness matrix in the FEM sense (relates the nodal point displacements to nodal point forces). Through Eq. (32), the linking of FEM with BEM can be achieved by using the transformation matrix $[M]$. More details about the linking of FEM with BEM are given in Ref. [35]. It should be noted that, since the matrix is obtained from BEM, the stiffness matrix is unsymmetrical. Thus, we can convert it to a symmetric matrix or use the symmetric equation solution capability of ABAQUS.

In the computation of the coupling scheme, the BEM domain can be treated as a finite element and its stiffness matrix $\mathbf{K}_{BE}$ can be evaluated by the above description.

4 Implementation of Coupling Scheme by ABAQUS

To make the current scheme more acceptable, we will introduce an automatic procedure to realize the coupling scheme. The software ABAQUS is currently one of the most powerful finite element analysis implementation in the world. On one hand, ABAQUS includes many kinds of material models and adaptive remeshing module. On the other hand, it is a powerful tool to solve some highly nonlinear problems. In this work, the coupling scheme described can be readily implemented in ABAQUS by making use of the UEL subroutine provided by ABAQUS. The technique that combines the BEM-code and the commercial finite element program ABAQUS is presented in Fig. 3. The numerical implementation process is as follows:

- The considered model is divided into FE and BE subdomains according to their geometric features or material properties.
- Then, two deformable parts should be built by ABAQUS: one is FE part and the other is the new-BE part. The FE part is built by a standard operation in ABAQUS. While the new-BE part is just one line (along the interface) and is called the effective BE part. The two parts are connected by the command 'tie'.
- After the FE part and effective BE part are built, the modeling procedure (including material data definition, meshing, and boundary condition application) for the coupled scheme is the same as a pure FE model.

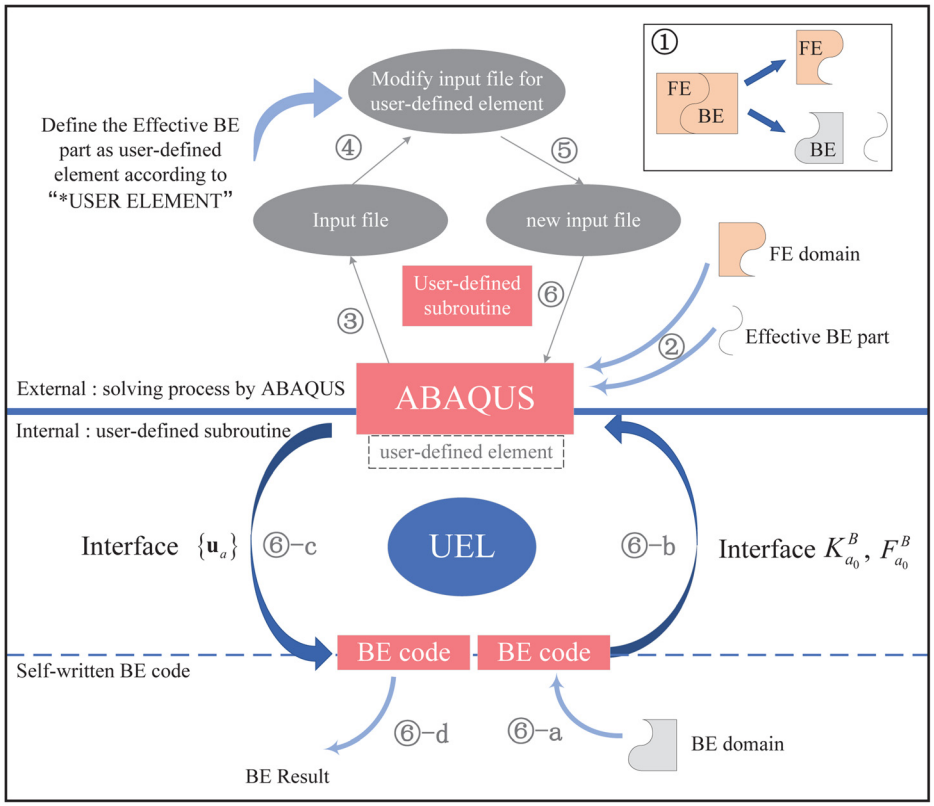

Fig. 3 The flowchart of coupling scheme

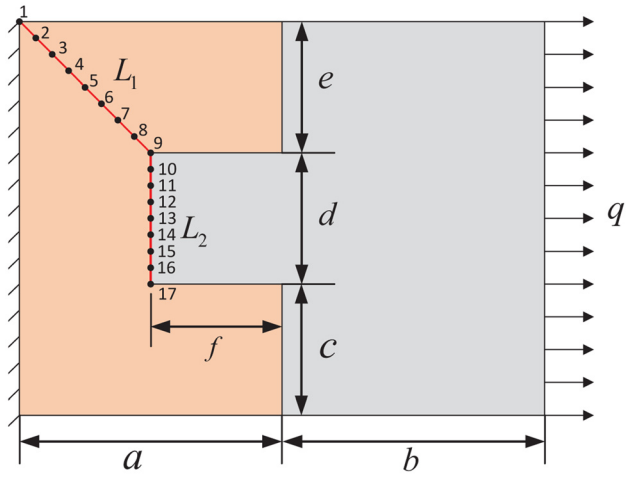

Fig. 4 Plane plate model under uniaxial tension

- The input file obtained by ABAQUS needs to be edited to define the effective-BE part as a user-defined element according to the user's manual of ABAQUS [36].
- After the above modeling procedure, we will import the input file into ABAQUS for the coupling numerical analysis.
- Based on the prepared input file, a new job is created. In the calculation, the user subroutine UEL including the self-written BEM code is then called to perform the coupling scheme. All the necessary BE data (nodes, boundary elements, geometry properties, materials, interfaces, boundary conditions) will be provided in the UEL. The effective initial nodal forces and stiffness matrix of the user-defined element can be obtained by the BE-code. Based on the above formulations and the obtained effective initial nodal forces and stiffness matrix, the final coupled equation will be formed.

5 Numerical Examples

In this section, several representative numerical examples are used to demonstrate the performance of the proposed coupling method. For a start, we focus on the accuracy and convergence

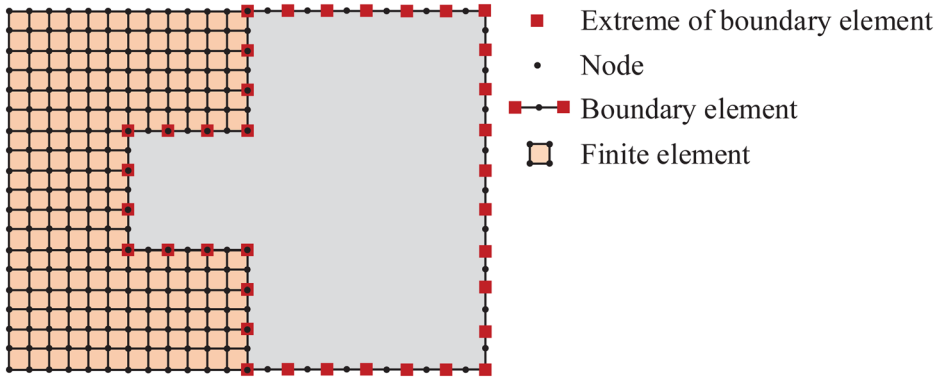

Fig. 5 Meshes used in the computation: quadrilateral element for FEM region and boundary element for BEM region

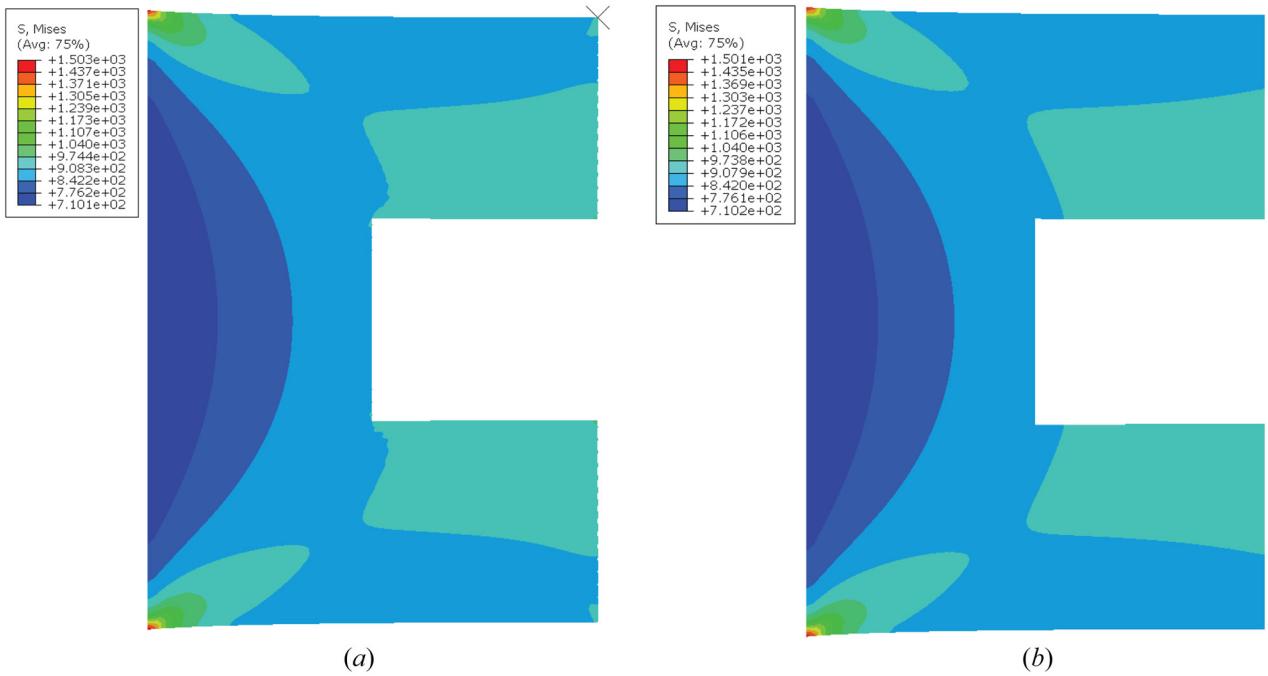

Fig. 6 von Mises stress contours computed by the present method and FEM: (*a*) contour of present results and (*b*) contour of FEM results

Table 1 Displacement results obtained by two methods for different n-DOFs

	Present solutions		Reference solutions	
Point index	n-DOFs = 930	n-DOFs = 3138	n-DOFs = 6626	n-DOFs = 396,292
1	0	0	0	0
2	0.23133	0.25111	0.25962	0.26226
3	0.45833	0.47683	0.48270	0.48391
4	0.67909	0.69706	0.70300	0.70391
5	0.89804	0.91761	0.92449	0.92556
6	1.11694	1.13946	1.14788	1.1496
7	1.33571	1.36243	1.37304	1.37626
8	1.55249	1.58521	1.59911	1.60559
9	1.83752	1.83756	1.83761	1.83766
10	1.83145	1.83146	1.83151	1.83155
11	1.82730	1.82728	1.82732	1.82736
12	1.82488	1.82485	1.82487	1.82491
13	1.82408	1.82404	1.82427	1.8241
14	1.82488	1.82485	1.82487	1.82491
15	1.82730	1.82728	1.82732	1.82736
16	1.83145	1.83146	1.83151	1.83155
17	1.83750	1.83755	1.83761	1.83766

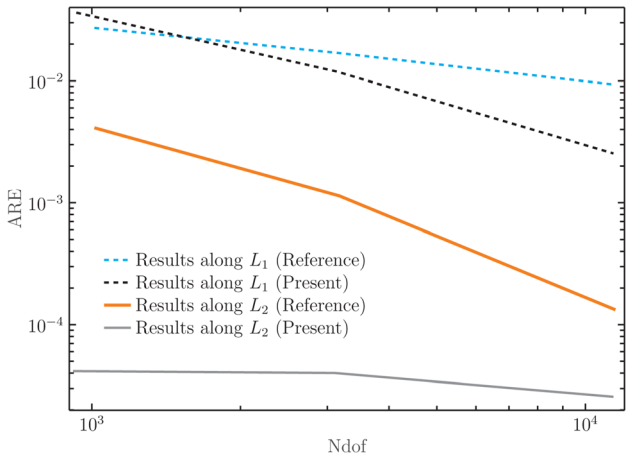

Fig. 8 Displacements convergence for different methods

analysis of the proposed coupling scheme. Then, the effectiveness of the method is illustrated by the comparison of the computation time and using memory for different methods. To further study the accuracy and effectiveness of the coupling method, we examine several physical problems in electronic packaging.

5.1 A Plane Plate Under Uniaxial Tension. To verify the accuracy of the proposed method, a plane plate with two regions under uniaxial tension is analyzed. Although the plane plate is a simple structure, it can be used to show strengths and weaknesses of the proposed method. As is shown in Fig. 4, the left side of the plate is fixed, i.e., $u_x = 0$ and $u_y = 0$. Geometric dimensions of the model are $a = b = 4$mm, $c = d = e = f = 2$mm. The right-hand side of the plate is subjected to a distributed load of $q = 1000\,\mathrm{N/mm}$ along the x direction. The material properties are assumed to be $E = 1000\,\mathrm{MPa}$ and $\nu = 0$. In the computation, the left part (shown in Fig. 4) is simulated by the finite element method and the boundary element method is used to study the right part.

For the boundary element region, quadratic element (three nodes per element) is used to describe the boundary geometry and physical quantities. To guarantee the identical interface nodes, four-node quadrilateral element is used for the descritization of finite element region. The meshes of the two regions are shown in Fig. 5, from which we can find that the number of elements used in the proposed coupling method is much less than that in a pure FEM analysis.

Here, a pure finite element model is constructed with the commercial software ABAQUS using a very refined mesh. The mesh consists of 198,146 nodes with 38,400 quadrilateral elements. Figures 6(*a*) and 6(*b*) show the von Mises stress distribution of the left part for the coupling method and reference solution. Figures 6(*a*) and 6(*b*) also imply that the accuracy of the present method is satisfactory in the whole field of the problem.

In order to study the convergence 283 of the numerical method, two sets of nodes ((a) 1–9 and (b) 10–17) along curves L_1 and L_2 (shown in Fig. 5) are selected and the displacements for different n-DOFs at these nodes are listed in Table 1. Figures 7(*a*) and 7(*b*) show the displacements (u_x) along curves L_1 and L_2 for different methods, respectively. From Table 1, Figs. 7(*a*) and 7(*b*) we can find that the results obtained by the present coupling method have a great agreement with the reference solutions. The convergence of the present solutions can be clearly seen even though the selected point lies on the interface boundary of two regions.

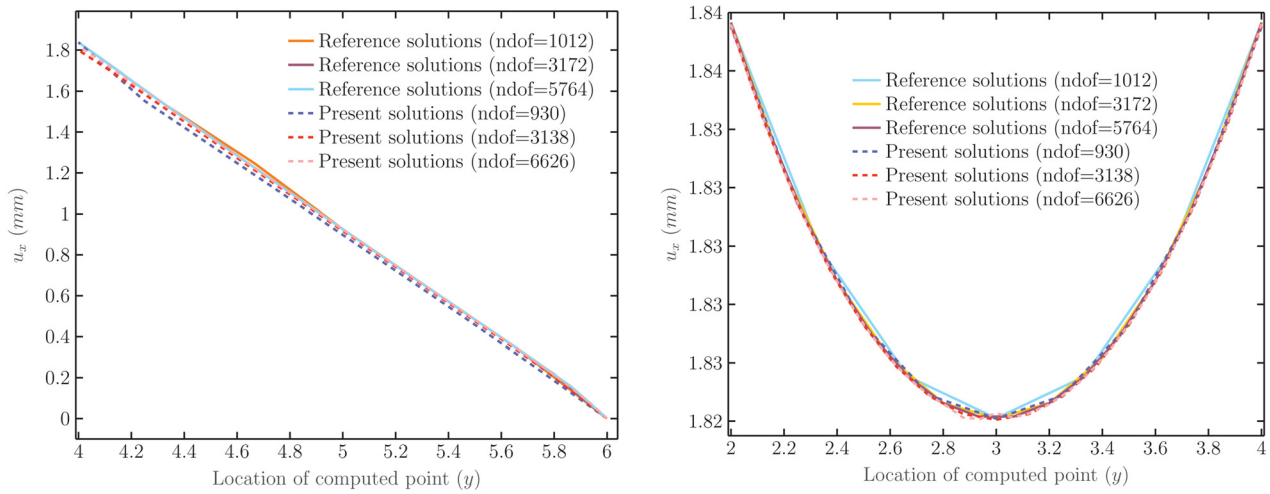

(*a*) (*b*)

Fig. 7 Displacements (u_x) obtained by different methods: (*a*) u_x along L_1 and (*b*) u_x along L_2

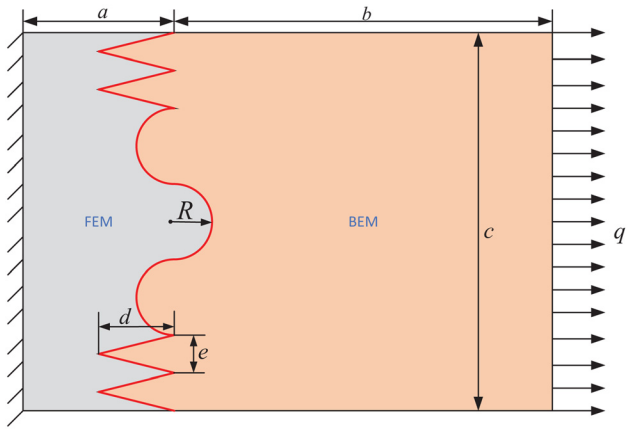

Fig. 9 Plane plate with complex interfaces

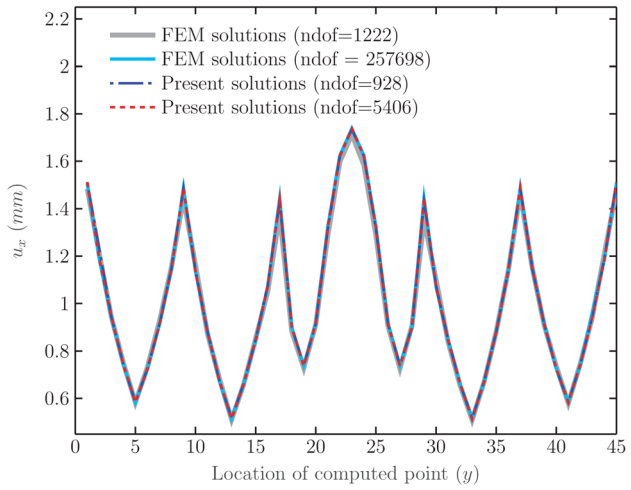

Fig. 10 Displacement (u_x) along the interface for different methods

For this model, the convergence of the problem is established by taking a very refined FEM model as the reference solution. Thus, we define an error metric

$$\text{Average relative error(ARE)} = \frac{1}{N}\sum_{i=1}^{N}\left|\frac{u^i_{\text{num}} - u^i_{\text{ref}}}{u^i_{\text{ref}}}\right| \tag{33}$$

where N is the number of evaluation points along lines L_1 and L_2 used to compute the error, and u^i_{num} (or u^i_{ref}) represents the numerical (or reference) result at the ith point. Figure 8 studies the convergence of the proposed method and a pure FEM (reference) when we refine the mesh for different locations (L_1 and L_2). For results along curve L_1, the convergence of the proposed method is demonstrated well with increasing n-DOF. The average relative errors obtained by the present method along the interface curve L_2 are small even when the n-DOF is less than 103 and remain stable as the number of degrees-of-freedom increases from 103 to 104. Although the convergence of the reference results obtained by a pure FEM can be seen, the average relative error is much higher than that evaluated by the proposed coupling scheme. The reason for this is that the boundary element results are used in the interface of the two regions. Again, we can find that the proposed coupling scheme gives some advantages over pure FEM in the computation accuracy.

5.2 Plane Plate With Different Materials and Complex Interfaces. Here, a 14 mm × 10 mm plane plate with different materials and complex interfaces is studied, as shown in Fig. 9. The geometry parameters of the model are given as $a = 4$ mm, $b = c = 10$ mm, $d = 2$ mm, $e = 2$ mm, $R = 2$ mm. The elastic modulus and Poisson's ratio of the left part and right part are given as $E_l = 3000$ MPa, $_l = 0.3$ and $E_r = 1000$ MPa, $\nu_r = 0.1$. As shown in Fig. 9, the end of the right part is subjected to a pressure of $q = 1000$ MPa, and the left surface of the left part is fixed. The tie constraint is imposed on the interface of the two parts. In the numerical analysis, the left part (FEM domain) is studied by FEM and the right part (FEM domain) is analyzed by BEM.

Figure 10 shows the numerical results of displacement (u_x) along the interface obtained by the present coupling method. In Fig. 10, results obtained by a pure FEM are also used as comparison. From the figure, it can be seen that the current results are in

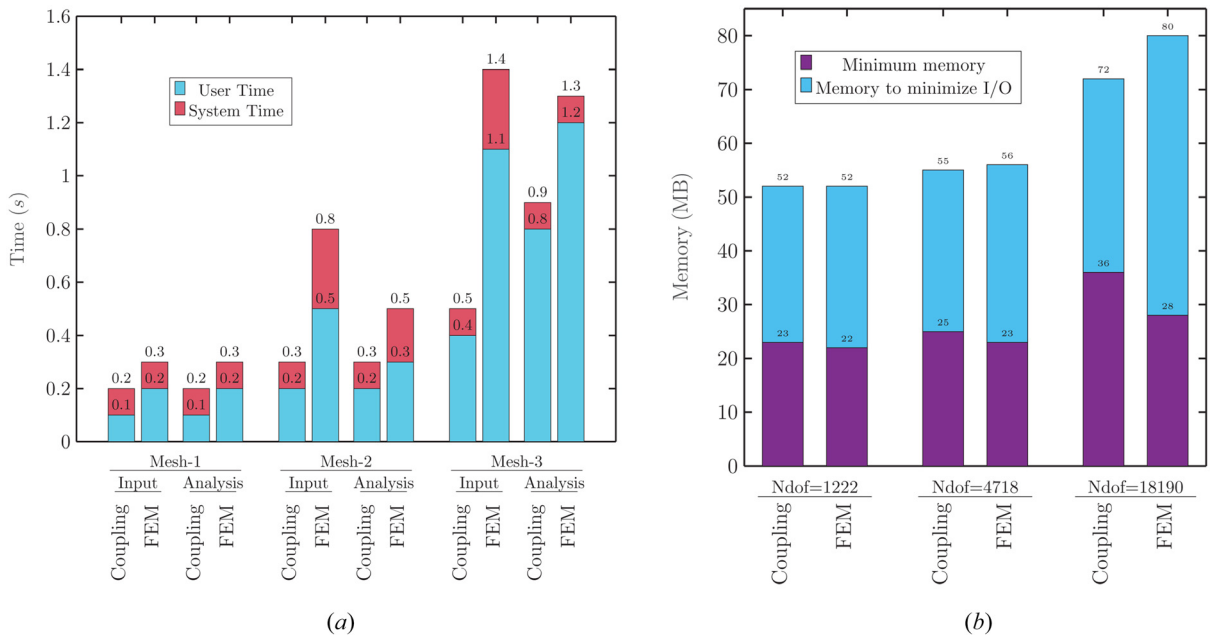

(a) (b)

Fig. 11 Computation time and memory comparison between the coupling method and pure FEM by ABAQUS: (*a*) time comparison and (*b*) memory comparison

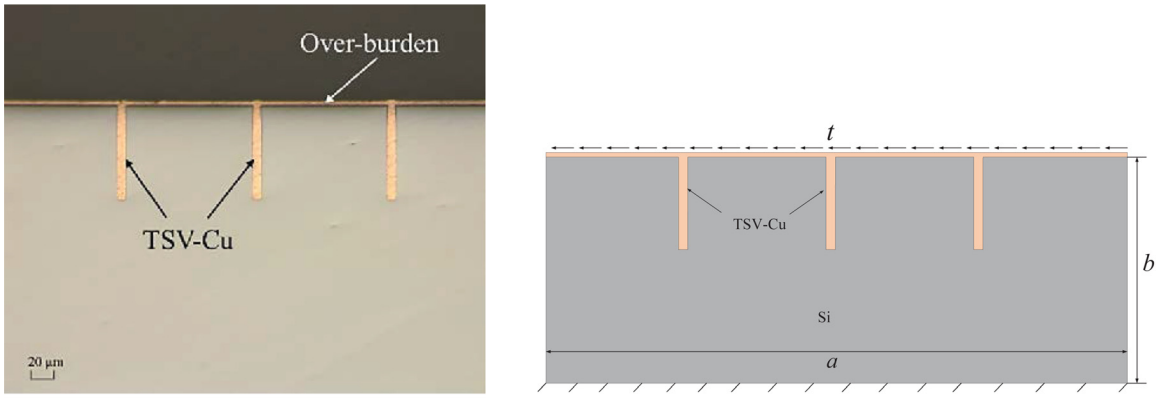

(*a*) (*b*)

Fig. 12 TSV model: (*a*) SEM image of TSV cross section and (*b*) schematic of TSV model

excellent agreement with the FEM results, even when the n-DOF equals 928 for current method and n-DOF = 257,698 for FEM solutions.

To study the effectiveness of current coupling scheme, Figs. 11(*a*) and 11(*b*) show the comparison of computational time and memory requirement between the proposed coupling method and a pure FEM. From the two figures, we can find that both the computational time and memory requirement of the two methods increase with the increasing of n-DOF. While the current coupling scheme requires less computational time and memory than that of

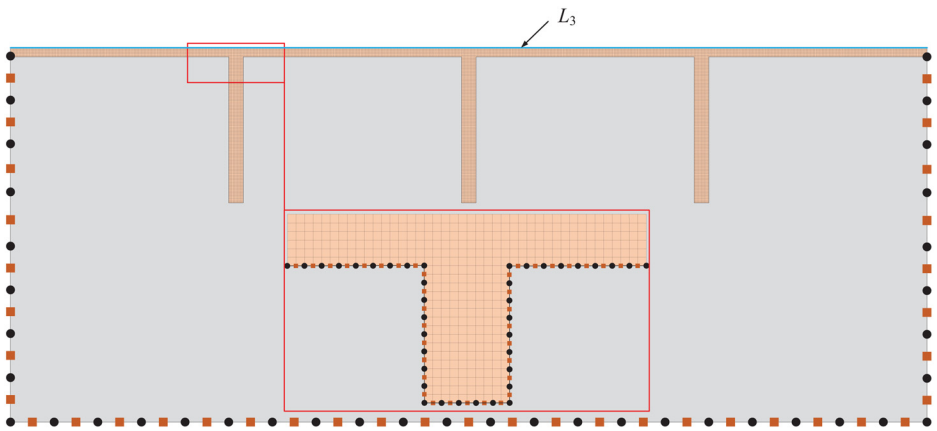

Fig. 13 Meshes used in the TSV model by using the coupling method

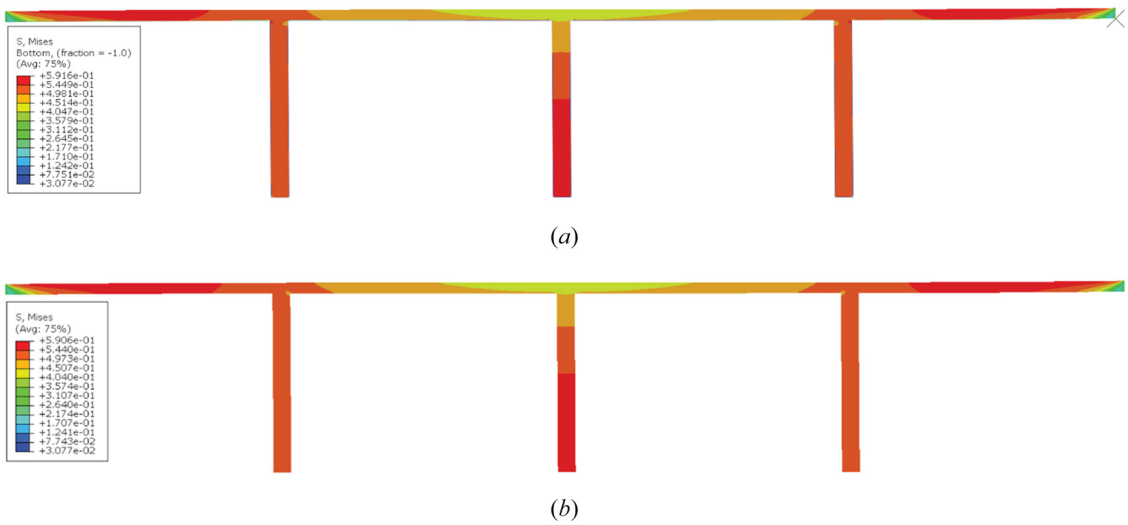

Fig. 14 Contour plot of von Mises stress: (*a*) results obtained by BEM and (*b*) results obtained by FEM

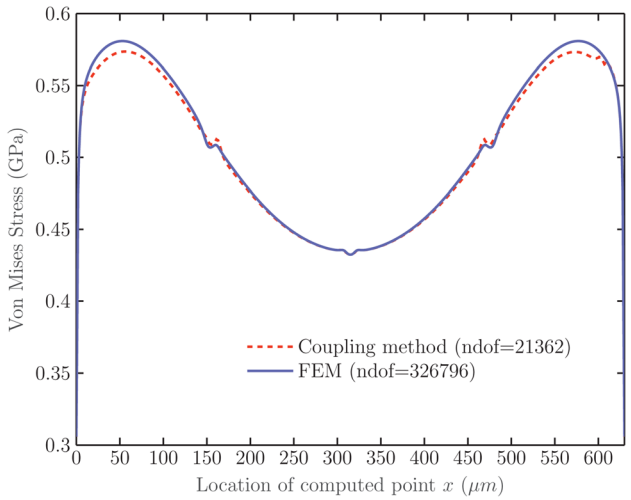

Fig. 15 The von Mises stresses at points lying on the contour L_3

FEM when same n-DOF is used. Since the level of approximation in the BE solution is confined to the surface, BE meshes should not be compared to FE meshes with the internal points removed. To achieve comparable accuracy in stress values, FE meshes would need more boundary divisions than the equivalent BE meshes. Therefore, the FEM-BEM coupling method can reduce the number of degrees-of-freedom for electronic packaging problems.

5.3 Through Silicon Via-Cu. To further study the application of the coupling method in real physical problems, a TSV-Cu (Through silicon via-Cu) model which is a promising technology in the 3D stacked packaging [37] is analyzed. Figure 12(*a*) shows a SEM image of TSV cross section and the mechanical properties of the TSV can be found in Ref. [37]. TSV-Cu is prepared by dry etching holes in silicon (Si) wafers and then filling them with

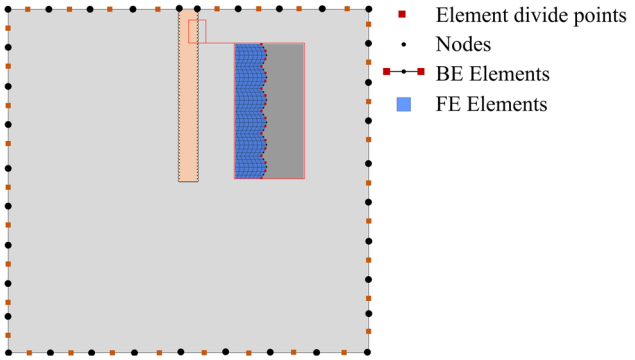

Fig. 17 Meshes used in the TSV model by using the coupling method

Copper (Cu) to achieve mechanical support and electrical interconnection of transistors. After the electroplating and filling process, Cu over-burden is usually retained on the surface. To form a smooth surface of low roughness, the over-burden needs to be removed.

In this example, a simplified 2D model (shown in Fig. 12(*b*)) is developed to study the stress and displacement distribution inside the TSV-Cu by using the coupling method. The diameter of TSV-Cu is 10 μm, and its depth is about 100 μm. The depth of the over-burden is 6 μm. In the numerical model, the geometry parameters a and b of Si are 630 μm $\times$ 250 μm, respectively. As shown in Fig. 12(*b*), the bottom of Si model is fixed (i.e., $u_x = u_y = 0$) and the surface of over-burden is subjected to shear traction $t = 0.25$ N/m. In the computation, the elastic modulus of Si and TSV-Cu used in this work are $E_{Si} = 140$ GPa and $E_{Cu} = 155$ GPa, respectively. The Poisson's ratio of Si and TSV-Cu are taken as $\nu_{Si} = 0.25$ and $\nu_{Cu} = 0.3$.

As introduced above, the numerical model will be divided into two regions, i.e., FE subdomain and BE subdomain. Due to the influence range of the subjected traction on the model being near the TSV-Cu, and the boundary condition has limited influence on the other domain. In the numerical analysis, the finite element

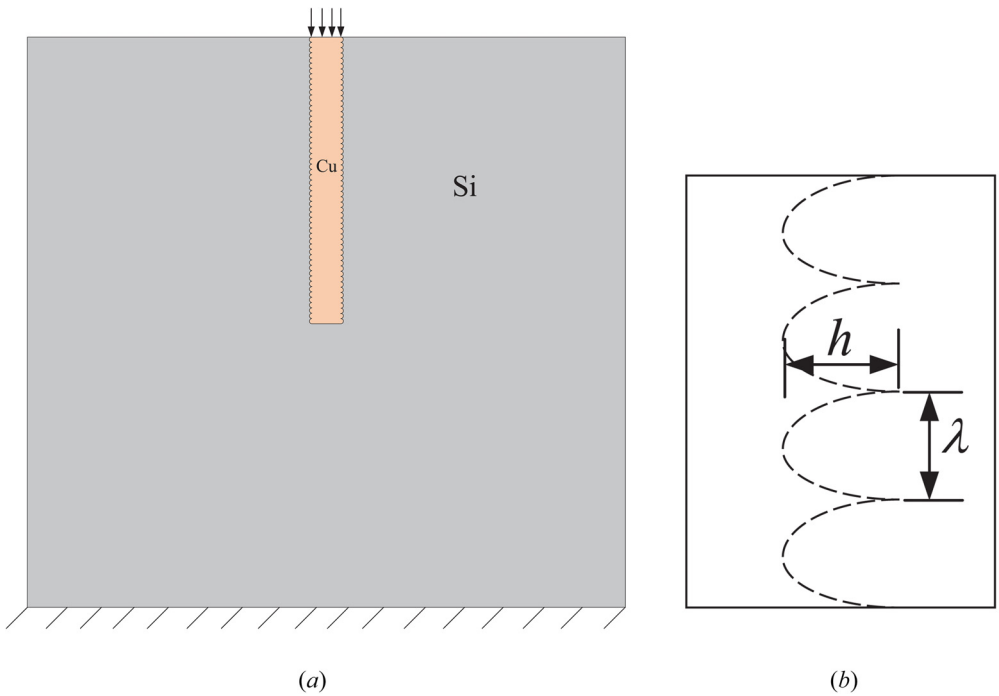

Fig. 16 The computed TSV-Cu/Si model: (*a*) model considering roughness of TSV-Cu/Si interface and (*b*) parameters of TSVCu/Si interface

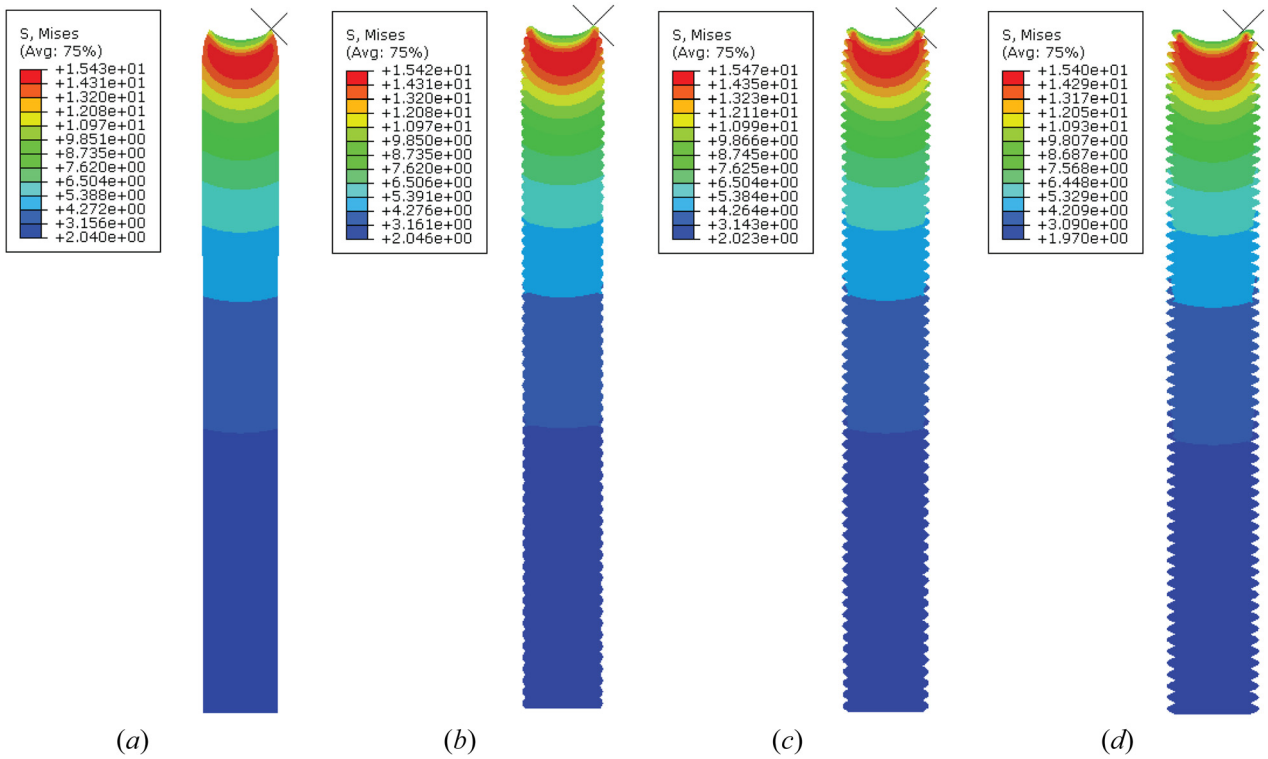

Fig. 18 von Mises stress contour plots in TSV-Cu: (*a*) $R^* = 0$, (*b*) $R^* = 0.25$, (*c*) $R^* = 0.50$, and (*d*) $R^* = 0.75$

method is used to study the TSV-Cu structure and the boundary element method is used to analyze the Si part. Figure 13 shows the meshes used in the coupling method, from which we can find that quadrilateral element is used in the TSV-Cu region and boundary element is used to discretize the boundary of Si region. We conclude that the number of elements used in the coupling scheme could be largely reduced.

Figure 14(*a*) shows the contour plot of the von Mises stresses in the TSV domain obtained by the proposed scheme. For comparison, the contour plot of FEM is provided in Fig. 14(*b*).

To further illustrate the accuracy of the current method to solve practical problem, we plot in Fig. 15 the von Mises stresses at points lying on the contour L_3, which is shown in Fig. 12(*b*). From Fig. 15, we can find that the results obtained by the proposed coupling method have a great agreement with that obtained by FEM.

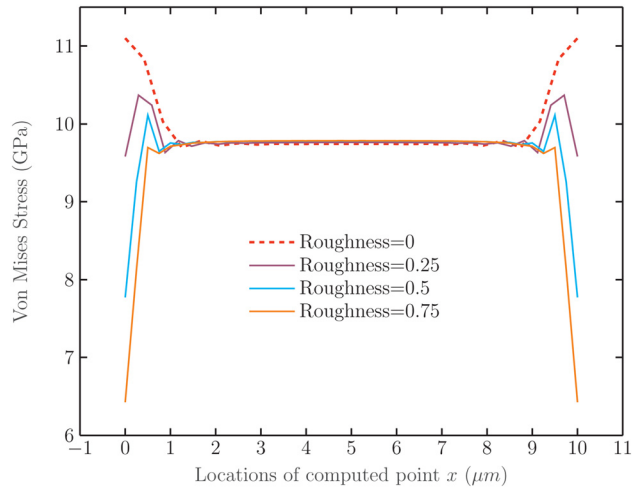

Fig. 19 von Mises stress along the interface of TSV-Cu/Si for different roughness ratios

6 Through-Silicon Via-Cu Structures With Different Interface Roughness

To further demonstrate the performance of the coupling method, a simplified TSV-Cu structure with different interface roughness (shown in Fig. 16(*a*)) is simulated in this section. More researches about interface roughness of TSV-Cu/Si can be found in Ref. [38]. In this paper, the problem is simplified as a 2D model, as shown in Figs. 16(*a*) and 16(*b*). To describe the interface roughness, we introduce the following dimensionless roughness ratio:

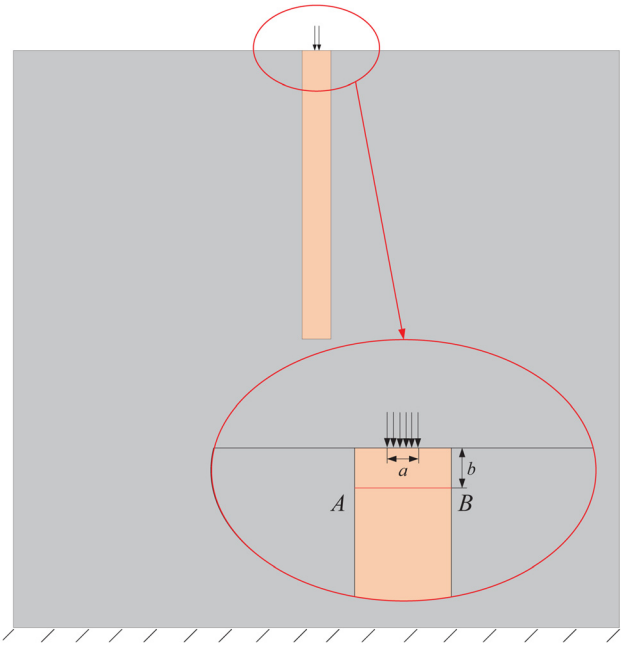

Fig. 20 Elastic-plastic model with $R^* = 0$

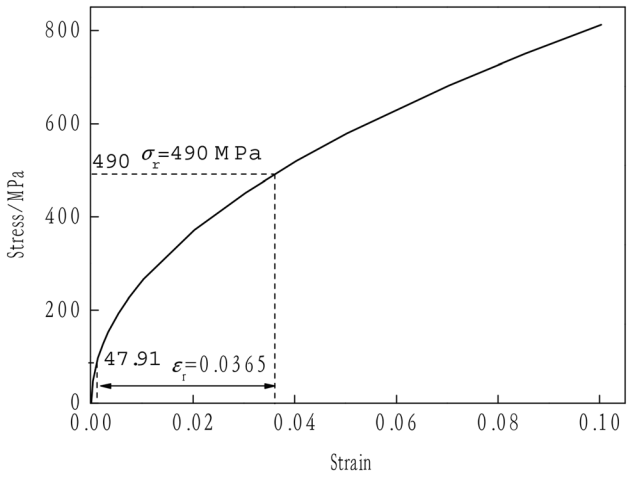

Fig. 21 Stress–strain relationship of TSV-Cu [39]

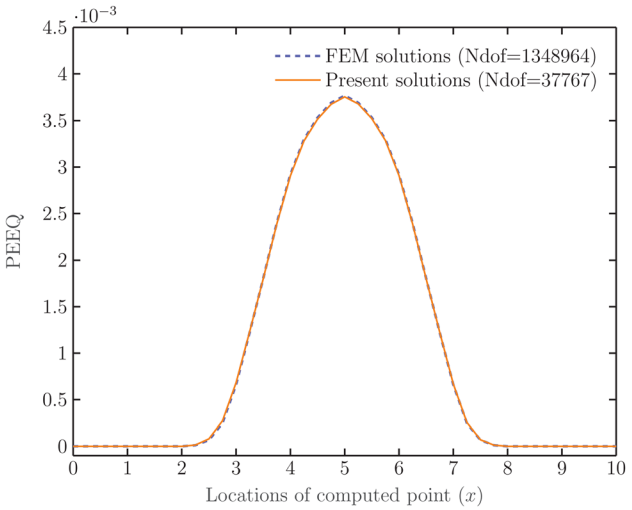

Fig. 23 PEEQs along line AB

$$\text{Interface roughness}(R^*) = \frac{h}{\lambda} \tag{34}$$

where λ represents the wavelength and h is the peak amplitude of the scalloped interface (as shown in Fig. 16(*b*)).

The material constants for this TSV-Cu model are the same as above. The diameter of TSV-Cu is 10 μm, and its depth is 100 μm. The geometry of Si domain is defined as 210 μm × 200 μm. The bottom side of Si region is fixed (i.e., $u_x = u_y = 0$) and the surface of TSV-Cu is subjected a uniform surface traction $f = 25\,\text{N/m}$. In the computation, the parameter h is taken as 0, 0.4, 0.8, and 1.2 and λ are fixed as 1.6 μm, which results in the roughness values of $R^* = 0, 0.25, 0$ and 0.75. Figure 17 shows the schematic of mesh used in proposed coupling scheme. From Fig. 17, we can find that the region of TSV-Cu is studied by FEM with (four-node element), and quadratic elements are used to discretize the boundary of BE subdomain (Si region).

Figures 18(*a*)–18(*d*) show the von Mises stress contour plots in TSV-Cu for different interface roughness. Meanwhile, the von Mises stress along interface of TSV-Cu under different interface roughness is shown clearly in Fig. 19. From these figures, we can clearly see the influence of the different interface roughness on the von Mises stress. As the interface roughness ratio increases, the stress on the surface of TSV-Cu decrease, especially at the connection area of two regions.

Actually, the coupling scheme is also applicable to elastic-plastic problems. Here, an elastic-plastic model with interface roughness ratio $R^* = 0$ is used to demonstrate the effectiveness of the proposed coupling method. As shown in Fig. 20, a part of the top surface (along the curve $a = 2$) of TSV-Cu is subjected to a

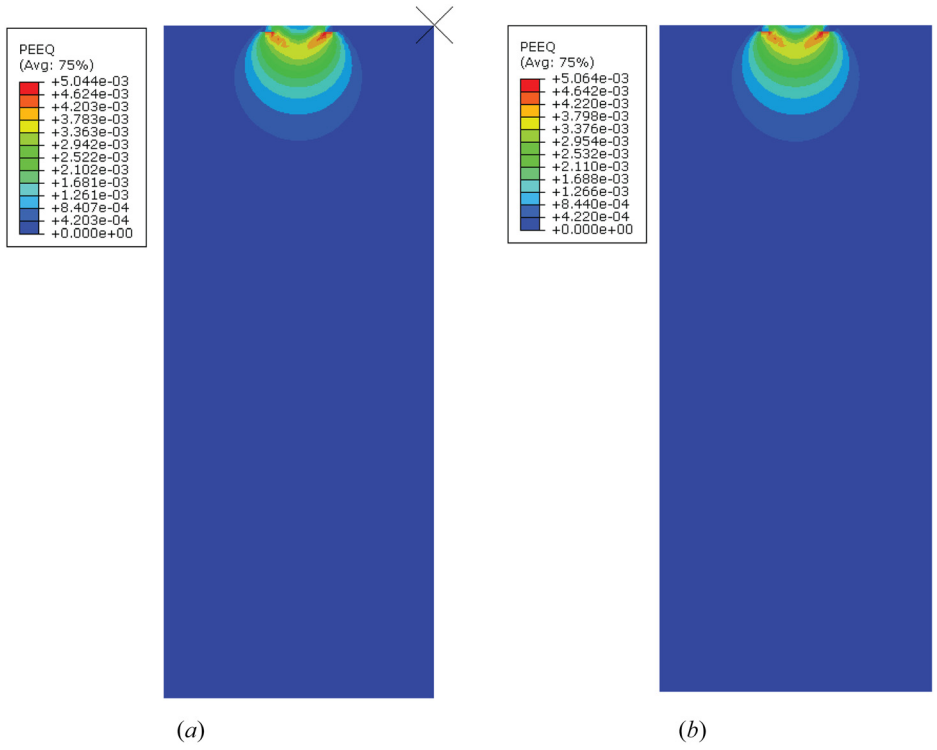

(*a*) (*b*)

Fig. 22 Equivalent plastic strains (PEEQ) contour plots in TSV-Cu by different methods: (*a*) PEEQ obtained by the coupling scheme and (*b*) PEEQ obtained by FEM

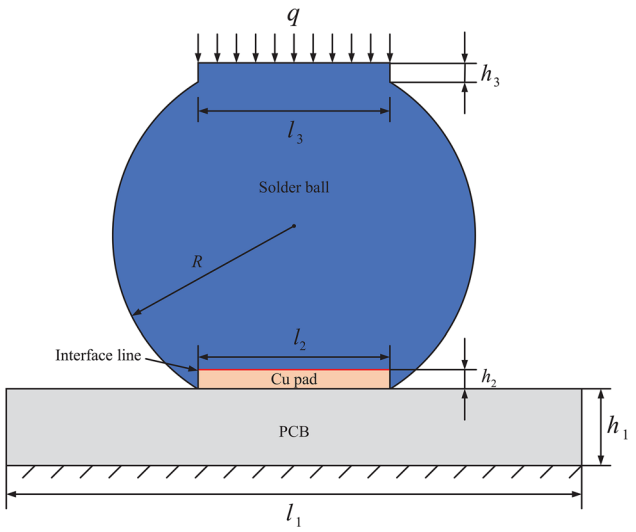

Fig. 24 BGA model

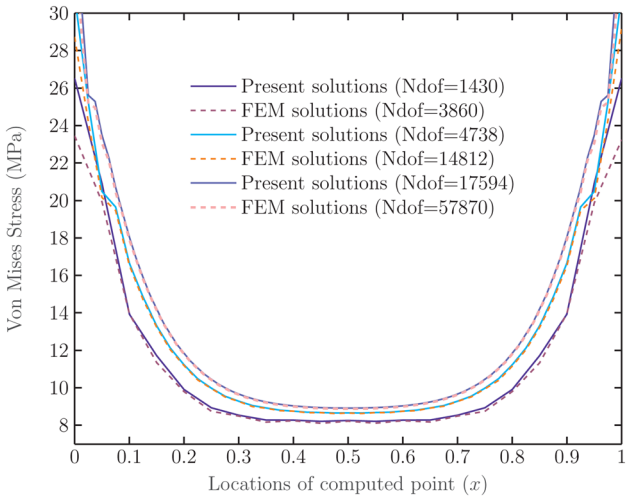

Fig. 26 von Mises stress distribution along the interface between Cu layer and solder ball

Table 2 Material parameters used in the computation

	Young's modulus E/Pa	Poisson's ratio v
PCB	22,000	0.15
Cu	110,000	0.35
Solder ball	10,000	0.4

surface traction $q = 0.2$ N/m. In the computation, Si is regarded as a linear elastic material, and TSV-Cu will be studied by an elastic-plastic model. The stress–strain relationship of TSV-Cu is from the following equation [39] and its stress–strain relationship is given in Fig. 21

$$\sigma = \begin{cases} 155,000\varepsilon, (\sigma \le 47.91\,\text{MPa}) \\ 11052.25\varepsilon_{\text{p}} + 47.91, (\sigma > 47.91\,\text{MPa}) \end{cases} \tag{35}$$

where the yield strength is 47.91 MPa and ε_p is the plastic strain.

Since ABAQUS is convenient and powerful for elastic-plastic problems, the TSV-Cu is studied by FEM in this model. That is to, say, the TSV part will be the FE region. The Si domain will be studied by BEM, which can largely reduce the number of elements. The values of PEEQ along the curve AB (shown in Fig. 20 with $b = 1$) are given in Fig. 23. From Figs. 22(*a*), 22(*b*), and 23, we can find that the results obtained by the proposed coupling method are in good agreement with the reference (FEM) results. The figures also imply that the proposed coupling method is effective for the elastic-plastic problem.

6.1 Ball Grid Array. In the final example, as shown in Fig. 24, a ball grid array (BGA) is used to show the stability of the coupling method. The geometry parameters are given as $l_1 = 3$ mm, $l_2 = l_3 = 1$ mm, $h_1 = 0.4$ mm, $h_2 = h_3 = 0.1$ mm and $R = 0.94$ mm. The material parameters are listed in Table 2. As shown in Fig. 24, the bottom of the printed circuit board (PCB) is fixed and the top of solder ball is subjected to a traction $t_y = 10$ N/m. In this example, FEM is used to analyze the PCB and Cu parts, and the solder ball is studied by BEM. The meshes used in the coupling method and FEM are shown in Figs. 25(*a*) and 25(*b*), respectively.

Figure 26 shows the von Mises stress distribution at the interface between Cu layer and solder ball obtained by the present coupling scheme and a pure FEM model. As shown in Fig. 26, there is an excellent agreement between the curves from the present coupling scheme and FEM. To further investigate the stability of the coupling scheme, the von Mises stress behavior at the interface is given in Fig. 27. In the computation, fixed n-DOF is used

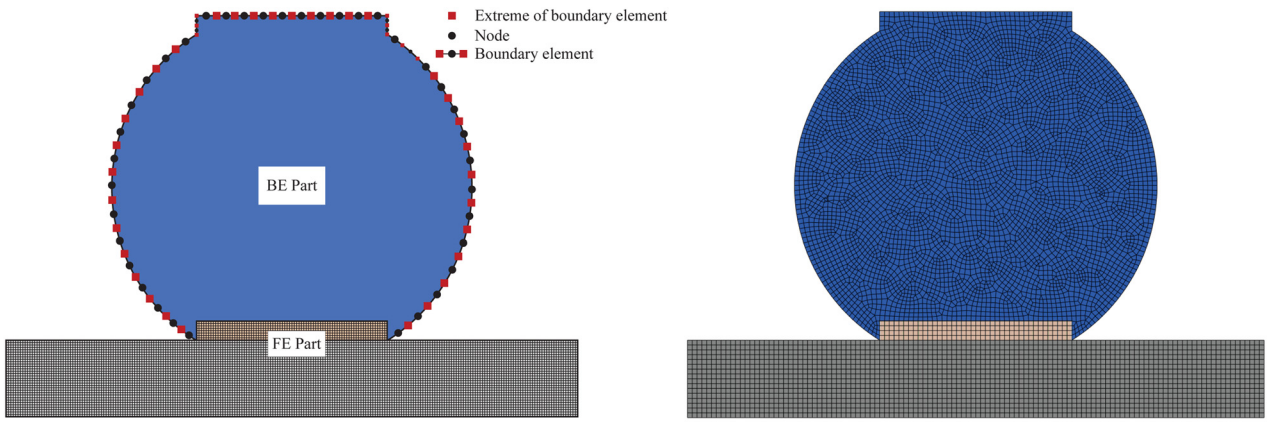

(*a*) (*b*)

Fig. 25 Comparison of mesh used in different methods: (*a*) mesh used in the coupling scheme and (*b*) mesh used in the FEM model

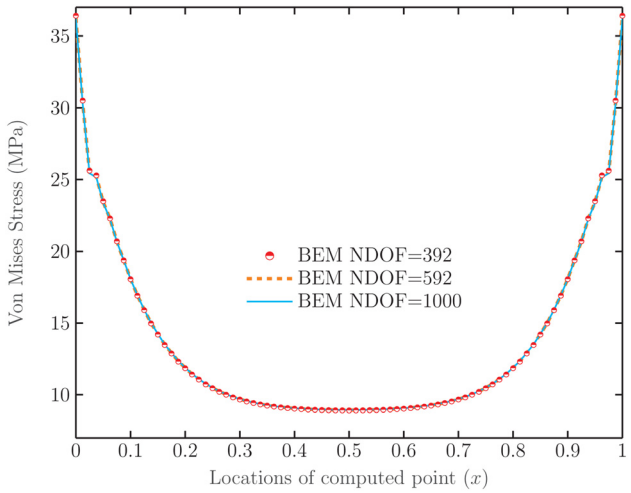

Fig. 27 von Mises stress distribution along the interface for different n-DOFs

in the FE-region and the n-DOF used in BE-region varies from 392 to 1000. These results demonstrate that the coupling method can obtain very accuracy results.

7 Conclusions

This paper presents an automatic procedure of the commercial finite element system ABAQUS with a self-written elastic boundary element code by using a UEL subroutine. In the implementation of the current coupling scheme, the numerical model is divided into the FE part and BE part. Obviously, FE part is studied by finite element method, and BE part is analyzed by boundary element method. BEM, regarded as an effective super-element is implemented in ABAQUS via UEL. The effective stiffness and effective tractions along the interface of BE and FE regions are evaluated by the self-written BE code. Application of the boundary conditions (including the obtained effective stiffness and effective tractions) then yields the final form of the FEM system through which the unknown quantities in the FE part can be obtained.

Using the advantages of both methods and avoiding their respective disadvantages, the coupling scheme allows user to study infinite and semi-infinite electronic packaging structures with local nonlinearities, stress concentration problems, and linear elastic fracture mechanics.

Acknowledgment

The authors thank editor Shi-Wei Ricky Lee and Jeffery C. C. Lo for the important help on the paper.

Funding Data

- National Natural Science Foundation of China (Grant Nos. 12002009 and 11872078; Funder ID: 10.13039/501100001809).
- General Program of Science and Technology Development Project of Beijing Municipal Education Commission (Grant No. KM202110005032; Funder ID: 10.13039/501100003213).

References

[1] Islam, N., Tan, K., Yoon, S. W., and Chen, T., 2019, "High Density Ultra-Thin Organic Substrates for Advanced Flip Chip Packages," IEEE 69th Electronic Components and Technology Conference (ECTC), Las Vegas, NV, May 28–31, pp. 325–329.

[2] Lederer, M., Gökdeniz, Z., Khatibi, G., and Nicolics, J., 2021, "Constitutive Equations for Strain Rate and Temperature Dependent Mechanical Behaviour of Porous Ag-Sintered Joints in Electronic Packages," Microelectron. Reliab., **126**, p. 114209.

[3] Alizadeh, R., and Mantooth, H. A., 2021, "A Review of Architectural Design and System Compatibility of Power Modules and Their Impacts on Power Electronics Systems," IEEE Trans. Power Electron., **36**(10), pp. 11631–11646.

[4] Mane, S. S., Soon, K. H., Bergmann, L., Erstling, M., Jayamani, E., and Patra, J., 2021, "Impact of Thermo-Mechanical Stress Due to Probing and Wire Bonding on Cup Devices," IEEE Trans. Compon., Packaging Manuf. Technol., **11**(8), pp. 1258–1266.

[5] Cheng, H.-E., and Chen, R.-S., 2014, "Interval Optimal Design of 3-D TSV Stacked Chips Package Reliability by Using the Genetic Algorithm Method," Microelectron. Reliab., **54**(12), pp. 2881–2897.

[6] Zhang, B., Shan, G., and Su, F., 2021, "Impact Reliability Analysis of a Rigid-Flex PCB System Under Acceleration Loads," Microelectron. Reliab., **127**, p. 114374.

[7] Xia, J., Cheng, L., Li, G., and Li, B., 2017, "Reliability Study of Package-On-Package Stacking Assembly Under Vibration Loading," Microelectron. Reliab., **78**, pp. 285–293.

[8] Yu, H., Guo, Y., Gong, Y., and Qin, F., 2021, "Thermal Analysis of Electronic Packaging Structure Using Isogeometric Boundary Element Method," Eng. Anal. Bound. Elem., **128**, pp. 195–202.

[9] Vallepuga-Espinosa, J., Ubero-Martínez, I., Rodríguez-Tembleque, L., and Cifuentes-Rodríguez, J., 2020, "A Boundary Element Procedure to Analyze the Thermomechanical Contact Problem in 3D Microelectronic Packaging," Eng. Anal. Boundary Elem., **115**, pp. 28–39.

[10] Khatir, Z., and Lefebvre, S., 2004, "Boundary Element Analysis of Thermal Fatigue Effects on High Power IGBT Modules," Microelectron. Reliab., **44**(6), pp. 929–938.

[11] Dong, C., and Lee, K. Y., 2008, "Stress Analysis of Plastic IC Package Containing Various Interface Delaminations Using the Boundary Element Method," Eng. Fract. Mech., **75**(1), pp. 1–16.

[12] Zienkiewicz, O. C., Kelly, D. W., and Bettess, P., 1977, "The Coupling of the Finite Element Method and Boundary Solution Procedures," Int. J. Numer. Methods Eng., **11**(2), pp. 355–375.

[13] Maljaars, P., Grasso, N., den Besten, J., and Kaminski, M., 2020, "BEM–FEM Coupling for the Analysis of Flexible Propellers in Non-Uniform Flows and Validation With Full-Scale Measurements," J. Fluids Struct., **95**, p. 102946.

[14] Gimperlein, H., Özdemir, C., and Stephan, E. P., 2020, "A Time–Dependent FEM-BEM Coupling Method for Fluid–Structure Interaction in 3D," Appl. Numer. Math., **152**, pp. 49–65.

[15] He, Z., Liu, G., Zhong, Z., Zhang, G., and Cheng, A., 2011, "A Coupled ES-FEM/BEM Method for Fluid–Structure Interaction Problems," Eng. Anal. Boundary Elem., **35**(1), pp. 140–147.

[16] Wu, H., Yu, L., and Jiang, W., 2019, "A Coupling FEM/BEM Method With Linear Continuous Elements for Acoustic-Structural Interaction Problems," Appl. Acoust., **150**, pp. 44–54.

[17] Pereira, M., Mareze, P., Godinho, L., Amado-Mendes, P., and Ramis, J., 2021, "Proposal of Numerical Models to Predict the Diffuse Field Sound Absorption of Finite Sized Porous Materials – BEM and FEM Approaches," Appl. Acoust., **180**, p. 108092.

[18] Wang, K., Liu, J., and Xu, J., 2022, "An Efficient FEM-BEM Solution for Electromagnetic Analysis of Inhomogeneous Objects," Eng. Anal. Boundary Elem., **134**, pp. 139–146.

[19] Rodopoulos, D. C., Gortsas, T. V., Tsinopoulos, S. V., and Polyzos, D., 2020, "Nonlinear BEM/FEM Scalar Potential Formulation for Magnetostatic Analysis in Superconducting Accelerator Magnets," Eng. Anal. Boundary Elem., **113**, pp. 259–267.

[20] Wang, J., and Huang, Q., 2020, "On Coupled FEM-BEM Simulation of the Magneto-Mechanical Behavior of Single-Crystalline Ni-Mn-Ga Alloys," Eng. Anal. Boundary Elem., **121**, pp. 143–157.

[21] Rodopoulos, D. C., Gortsas, T. V., Polyzos, K., and Tsinopoulos, S. V., 2019, "New BEM/BEM and BEM/FEM Scalar Potential Formulations for Magnetostatic Problems," Eng. Anal. Boundary Elem., **106**, pp. 160–169.

[22] Liravi, H., Arcos, R., Clot, A., Conto, K. F., and Romeu, J., 2022, "A 2.5D Coupled FEM–SBM Methodology for Soil–Structure Dynamic Interaction Problems," Eng. Struct., **250**, p. 113371.

[23] Ai, Z. Y., and Chen, Y. F., 2020, "FEM-BEM Coupling Analysis of Vertically Loaded Rock-Socketed Pile in Multilayered Transversely Isotropic Saturated Media," Comput. Geotech., **120**, p. 103437.

[24] Luamba, E. S., and de Paiva, J. B., 2022, "Static Analysis of Axially Loaded Piles in Multilayered Soils Using a BEM/FEM Formulation," Eng. Anal. Boundary Elem., **135**, pp. 63–72.

[25] Liu, Z., and Dong, C., 2016, "Automatic Coupling of ABAQUS and a Boundary Element Code for Dynamic Elastoplastic Problems," Eng. Anal. Boundary Elem., **65**, pp. 147–158.

[26] Sharma, N., Ranjan Mahapatra, T., Kumar Panda, S., and Mazumdar, A., 2018, "Acoustic Radiation Characteristics of un-Baffled Laminated Composite Conical Shell Panels," Mater. Today: Proc., **5**(11), pp. 24387–24396.

[27] Helldörfer, B., Haas, M., and Kuhn, G., 2008, "Automatic Coupling of a Boundary Element Code With a Commercial Finite Element System," Adv. Eng. Software, **39**(8), pp. 699–709.

[28] Qin, F., He, Q., Gong, Y., An, T., Chen, P., and Dai, Y., 2022, "The Application of FEM-BEM Coupling Method for Steady 2D Heat Transfer Problems With Multi-Scale Structure," Eng. Anal. Boundary Elem., **137**, pp. 78–90.

[29] Yang, Z., Yao, F., and Huang, Y., 2020, "Development of ABAQUS UEL/VUEL Subroutines for Scaled Boundary Finite Element Method for General Static and Dynamic Stress Analyses," Eng. Anal. Boundary Elem., **114**, pp. 58–73.
[30] Hetnarski, R., and Ignaczak, J., 2006, "Mathematical Theory of Elasticity," J. Therm. Stress., **29**(5), pp. 505–506.
[31] Zienkiewicz, O. C., Taylor, R. L., and Zhu, J. Z., 2013, *The Finite Element Method: Its Basis and Fundamentals*, Butterworth-Heinemann, Oxford, UK.
[32] Gong, Y., Dong, C., Qin, F., Hattori, G., and Trevelyan, J., 2020, "Hybrid Nearly Singular Integration for Three-Dimensional Isogeometric Boundary Element Analysis of Coatings and Other Thin Structures," Comput. Methods Appl. Mech. Eng., **367**, p. 113099.
[33] Hong, H., and Chen, J., 1988, "Derivations of Integral Equations of Elasticity," J. Eng. Mech., **114**(6), pp. 1028–1044.
[34] Chen, J. T., and Hong, H.-K., 1999, "Review of Dual Boundary Element Methods With Emphasis on Hypersingular Integrals and Divergent Series," Appl. Mech. Rev., **52**(1), pp. 17–33.
[35] Beer, G., Smith, I., and Duenser, C., 2008, *The Boundary Element Method With Programming: For Engineers and Scientists*, Springer, Vienna, Austria.
[36] Simulia D., 2011, *Abaqus 6.11 Analysis User's Manual*, Abaqus 6.11 Documentation.
[37] Li, Y., Chen, P., Qin, F., An, T., Dai, Y., Zhang, M., and Jin, Y., 2021, "Constitutive Modelling of Annealing Behavior in Through Silicon Vias-Copper," Mater. Charact., **179**, p. 111359.
[38] Chen, S., Wang, Z., En, Y., Huang, Y., Qin, F., and An, T., 2018, "The Experimental Analysis and the Mechanical Model for the Debonding Failure of TSV-Cu/Si Interface," Microelectron. Reliab., **91**, pp. 52–66.
[39] Qin, F., Xiang, M., and Wu, W., 2014, "The Stress-Strain Relationship of TSV-Cu Determined by Nanoindentation," Acta Metall. Sin., **50**(6), p. 722.